Oceanologia (2016) 58, 264—271

Available online at www.sciencedirect.com

ScienceDirect

journal homepage: www.journals.elsevier.com/oceanologia/

ORIGINAL RESEARCH ARTICLE

Detecting imprints of atmospheric waves in the Bering Sea with MODIS data

Marina Evdoshenko *

P.P. Shirshov Institute of Oceanology, Russian Academy of Sciences, Moscow, Russia

Received 11 November 2015; accepted 13 April 2016
Available online 29 April 2016

KEYWORDS
MODIS;
Remote sensing;
Ocean optics;
Water leaving radiance

Summary Satellite Moderate Resolution Imaging Spectroradiometer (MODIS) data of water leaving radiance of 859 nm with a spatial resolution of 250 m were used to investigate the impact of atmospheric gravity waves (AGWs), which manifested as stripes in clouds and on the sea surface. On the basis of an evaluation of the characteristics of AGWs and sea depth, it was shown that the surface stripes, or surface waves (SWs) were imprints of AGWs. Crests of SWs were like prolongations of cloud stripes on the combined radiance images testifying that SWs were shifted by minus a quarter of the period relative to AGWs.

1. Introduction

The possibility of processing the increased spatial resolution (250 m) data from Moderate Resolution Imaging Spectroradiometer (MODIS) has opened up new prospects (Franz et al., 2006). Particularly they concern more detailed observation of imprints of atmospheric phenomena, such as fronts, gravity waves, rain cells, convective cells and others, on the oceans' surface.

Atmospheric phenomena are usually invisible. Near infrared and optical radiance do not penetrate through clouds. However, at sufficiently high humidity atmospheric events can imprint in clouds and become visible on images of the radiance $L_t(\lambda)$ at the top of the atmosphere of level L1 (without the atmospheric correction). So, in the case of atmospheric gravity waves (AGWs), they display as “cloud streets” on $L_t(\lambda)$ images.

Atmospheric processes, that cause the variability of sea surface roughness, are usually investigated by their footprints on the sea surface with the help of satellite Synthetic Aperture Radar (SAR). Passive microwave radiation penetrates through clouds into the sea by no more than several millimeters so that surface snapshots of atmospheric impacts form SAR backscatter return (Valenzuela, 1978). Many papers

* Correspondence to: P.P. Shirshov Institute of Oceanology, Russian Academy of Sciences, 36, Nakhimovski prospect, Moscow 117997, Russia. Tel.: +7 4991245983; fax: +7 4991245983.
E-mail address: maarsio@bk.ru.
Peer review under the responsibility of Institute of Oceanology of the Polish Academy of Sciences.

ELSEVIER Production and hosting by Elsevier

http://dx.doi.org/10.1016/j.oceano.2016.04.003

are devoted to investigating atmospheric processes with the help of SAR, e.g. Alpers and Brummer (1994), Alpers and Huang (2011), Kozlov et al. (2014), Li et al. (2011), Vachon et al. (1994), Zheng et al. (1998).

In many published papers, atmospheric processes shown as cloudy structures have been examined in different geographical regions on the basis of MODIS true color $L_t(\lambda)$ images with a resolution of 250 m. Papers mentioned below contain some examples of signatures of atmospheric internal waves, coastally trapped atmospheric gravity waves, atmospheric vortex streets, atmospheric boundary rolls and convective cells: Da Silva and Magalhaes (2009), Liu et al. (2004), Li et al. (2008), Weigen et al. (2008).

One of the atmospheric impacts namely atmospheric gravity waves (AGWs) accompanied by corresponding changes in pressure, periodically force through the sea surface, modulating its level. This leads to a change in the normalized water leaving radiance $L_w(\lambda)$ (or remote sensing reflectance $Rrs(\lambda)$, which differs from $L_w(\lambda)$ by a factor of F_0 – mean solar irradiance) of level L2 (after the atmospheric correction). Under a clear sky, imprints of AGWs display on L_w images with sufficiently high resolution in the form of stripes of alternating brightness.

We have not found any papers where 250-m L_w images, obtained with MODIS, were used for identification of AGW signatures on the sea surface as surface waves (SWs). Also, we have not found any papers where a comparison of imprints of AGWs as cloud stripes on images of L_t and on the sea surface on images of L_w for a case of intermittent cloudiness was fulfilled on a single satellite picture. Therefore, the goal of this study was to obtain simultaneous 250-m MODIS images of AGW imprints in cloud and on the sea surface for some cases of their bright manifestations in different ocean regions. On the basis of an evaluation of a phase speed and a wavelength of AGWs, and water depth, we aimed to prove that found SWs were exactly imprints of AGWs, but not long surface gravity waves, and to reveal a phase shift between AGWs in cloud and the crests of SWs.

2. Material and methods

It is known that "normalized water-leaving radiance is that which would exit the sea surface if the Sun were at the zenith and if the atmosphere were absent" (Gordon et al., 1988). A layer width in which $L_w(\lambda)$ is formed varies with λ and is defined by the spectral dependence of the backscatter and the absorption coefficients of pure water and admixture.

Most MODIS optical radiance bands have spatial resolutions of 1 km, and only two bands I – at 645 nm and II – at 859 nm provide the resolution of 250 m. In clear ocean waters, $L_w(645)$ originates in a subsurface layer of 1–2 m, while $L_w(859)$ originates in the thin, topmost layer of about several centimeters due to the high absorption of pure water (Hale and Querry, 1973; Pegau et al., 1997). Our experience shows that imprints of atmospheric waves of small amplitude (up to some tens centimeters) are reproduced better by $L_w(859)$, than by $L_w(645)$ so we used only $L_w(859)$ data for our investigation.

Level L1a radiance MODIS data were obtained from http://oceancolor.nasa.gov, NOAA AVHRR L1 data – from http://www.class.ncdc.noaa.gov. MODIS level 2 radiance data were generated from level L1 data with the help of the SeaDAS software package, available on http://seadas.gsfc.nasa.gov. The process to generate 250-m data consists of several steps: obtaining a GEO file, generation of an L1b file and then generation of an L2 file, which includes radiance data and some product data, such as wind speed and direction. Wind components at a height of 10 m above the ocean were calculated for a given place and time by interpolating ancillary NCEP (National Centers for Environmental Prediction) data with the SeaDAS. Brightness and contrast of radiance images were enhanced slightly for better discernibility of AGWs in clouds and SWs.

3. Results

3.1. AGW packet in the Bering Sea

Optical scanners record imprints of AGWs on the ocean surface permanently (Evdoshenko, 2008, 2009). Consider their pronounced manifestations in the Bering Sea near St. Lawrence Island.

Appearance of cloud imprints in the Bering Sea at 22:45 on 6 June 2001 was caused by atmospheric solitary waves in the vicinity of St. Lawrence Island. That AGW packet propagating in the upwind direction was initially discovered in RADARSAT SAR image of arched atmospheric wave imprint on the sea surface and 250-m MODIS L_t-image of cloud waves (Li et al., 2004).

On 6 and 7 June 2001, the packet of quasi-stationary (standing) atmospheric waves was revealed as bow-shaped cloud stripes on several images of L_t of level L1 obtained from different satellite devices, including NOAA 14 AVHRR (Advanced Very High Resolution Radiometer), Terra MODIS (NASA's Earth Observing System – EOS AM) and OrbView-2 SeaWiFS (Sea-Viewing Wide Field-of-View Sensor). Images of standing atmospheric wave imprints in cloud, obtained from AVHRR at λ = 10.8 μm with a spatial resolution of 1 km, from MODIS at λ = 859 nm with resolution of 250 m and from SeaWiFS at λ = 670 nm with resolution of 1.1 km are shown in Fig. 1. One can see that the packet of AGWs existed for more than 10 h from the evening of 6 June up to the early morning of 7 June 2001.

The absence of the atmospheric cloud wave packet on AVHRR images of L_t at observations during the previous and following revolution periods of NOAA-14, each of which is equal to ~1 h 40 min, relative to the considered period of ~10 h, testified that the standing waves originated and disappeared rather abruptly. That is, solitary AGWs were formed only when the island was under the influence of the air break which propagated at low height.

St. Lawrence Island is 145 km long and 13–36 km wide. The highest mountain, with a maximum height H = 2207 m, is located in the middle of the island. Several mountains in its eastern part and a mountain at its western part are of lesser heights. Between the mountains are plateaus with numerous lagoons. Solitary, bow-shaped AGWs were obviously generated when the mountains blocked the cold arctic air break so that upstream waves arose as a secondary reflected flow. While passing freely through the plateaus to the leeward side of the island a part of the cold air break ramified and propagated downstream as cloud tails modulated by AGWs. On the lee side of the island cloudy AGWs turned around and moved downstream close to the meridian.

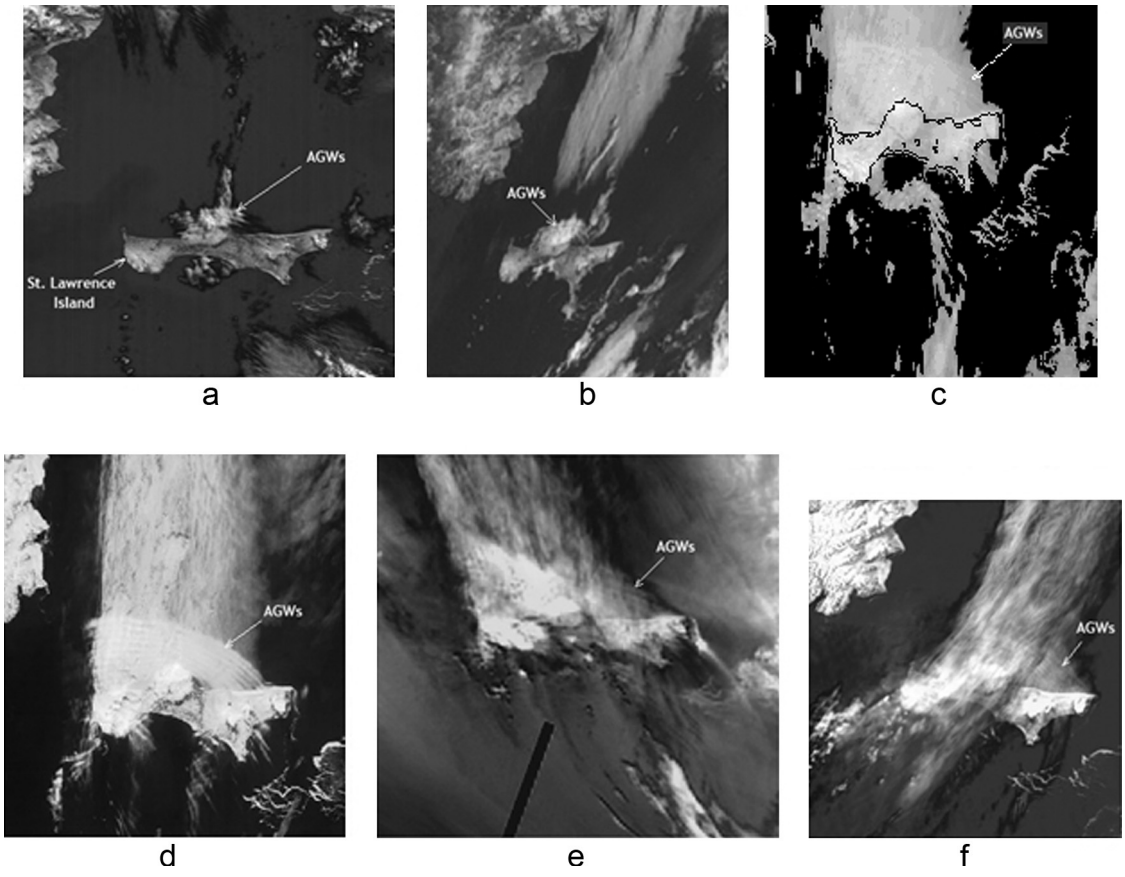

Figure 1 L_t-images from AVHRR at 17:15 on 6 June (a), AVHRR at 18:55 on 6 June (b), MODIS at 22:45 on 6 June (c), SeaWiFS at 0:35 on 7 June (d), AVHRR at 1:32 on 7 June (e) and AVHRR at 3:14 on 7 June (f).

An arctic cyclone, passing from the Arctic Ocean to the Bering Sea in the Pacific Ocean and provoking the movement of a cold air break to the south, was observed at 17:15 on 6 June on a MODIS 1-km image of L_t at 6.7 μm (channel 27). L_t(6700), reflecting the water vapor content at a height of 4.2 km (air pressure 600 hPa) showed that the northern tail end of the cyclone drew the cold air from the Arctic Ocean to St. Lawrence Island, the core of the cyclone being southward between St. Lawrence Island and the Aleutian Islands (see Fig. 2a).

Fig. 2b represents an enlarged MODIS L_t(859) image for the island surroundings. The AGW packet was revealed to the north and above the island as bow-shaped cloud stripes that were stretched from one end of the island to the other and resembled the island's arched southern boundary. The packet contained more than ten solitary waves, and the soliton wavelength was 4.75 km. To the south of the island several cloud tails appeared, consisted of a number of shorter, nearly linear cloud stripes that looked like a prolongation of the

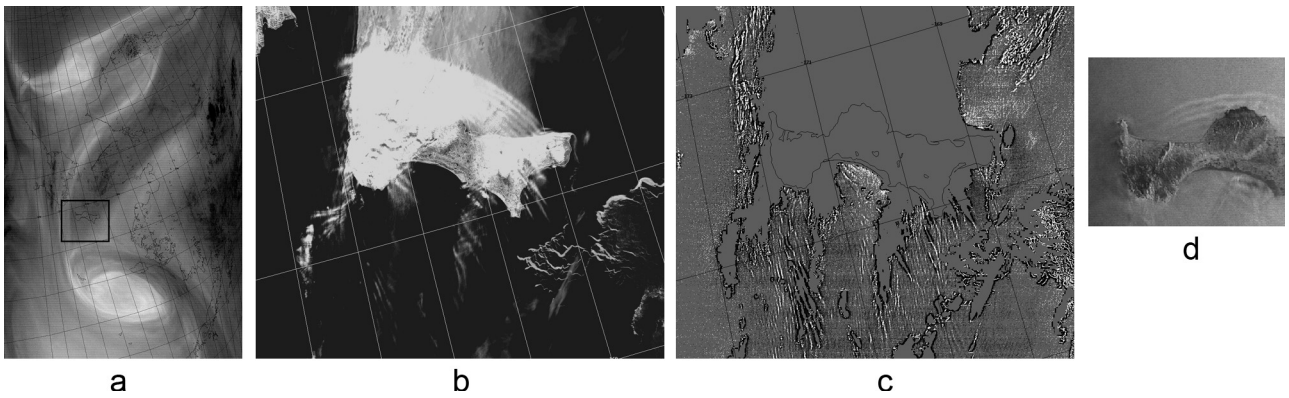

Figure 2 MODIS images at 22:45 on 6 June 2001: 1-km L_t(6700) (a), 250-m L_t(859) (b) and 250-m L_w(859) (c); coordinates of the box shown on (a) and regions shown on (b) and (c): 62.73°N, 174.14°W–63.97°N, 167.49°W; a RADARSAT ScanSAR wide B mode SAR image, acquired at 18:07:58 on 6 June 2001 (Li et al., 2004) (d).

arched waves to the north of the island. At the bottom right hand corner of Fig. 2b one can see a glacier.

The L_w(859) image shows AGW imprints as mainly longitude-oriented stripes of alternating brightness (or surface waves) southward of the island (see Fig. 2c). In contrast to the cloudy atmospheric wave appearance, when only one cloud stripe per period is visible, two stripes per period (light and dark) are visible in the case of surface imprints. The bright stripes symbolize wave crests, the dark ones symbolize wave troughs, the bright stripes being like continuations of cloud waves recognized on the L_w image as smooth gray stripes with pointed ends. Sea surface signatures that appeared as a great number of contrasting quasi-parallel stripes of different lengths and wavelengths were observable to the south of the island, at distances several times as great as the width of the island and attenuated with the distance. Their crest length reached hundreds of kilometers. Far from the island their wavelength decreased and was much smaller than that of the cloud arched waves to the north of the island. The minimum wavelength and the distinguishable crest width were limited by the scanner resolution, but undoubtedly signatures of lesser wavelength existed. Their crests are marked by dots instead of wider solid lines on Fig. 2c. To the south of the island, wavelengths of surface waves changed from ~1.5 km to ~4 km. Black boundaries on the image that restricted cloud areas can be explained by decreased values of L_w(859). They were obviously caused by the faults of the atmospheric correction.

A RADARSAT-1 SAR image of sea surface imprints of atmospheric waves with 100-m resolution, obtained at 18:07:58 on 6 June 2001, and presented in Li et al. (2004), is shown in Fig. 2d. On the image, imprints of AGWs on the sea surface in the form of arched waves to the north of the island are seen. Also visible are some signatures to the south from the island which coincide in direction with those appeared on MODIS L_w(859) image.

Fig. 3 represents L_t and L_w images of two smaller AGW packets in clouds and surface wave packets to the north and south from the island in the expanded scale. To the north from St. Lawrence Island arrows indicate a large, arched standing wave packet (LAGW), a smaller atmospheric wave packet (AGW) and a smaller SW packet. A smaller AGW packet propagated at an angle to the large, arched northern AGW packet (LAGW) and was evidently caused by a vertical velocity shear. Several tens waves are observable in the smaller, north-eastern AGW packet. The width of the packet is no less than 19 km, the wave crest length is no less than 3.4 km, and the wavelength is 0.9 km.

At the bottom of the L_t image, two wider AGW signatures of the bow-shaped packet (LAGW) are seen, and also surface waves (LSW) caused by them near the island's southern shore.

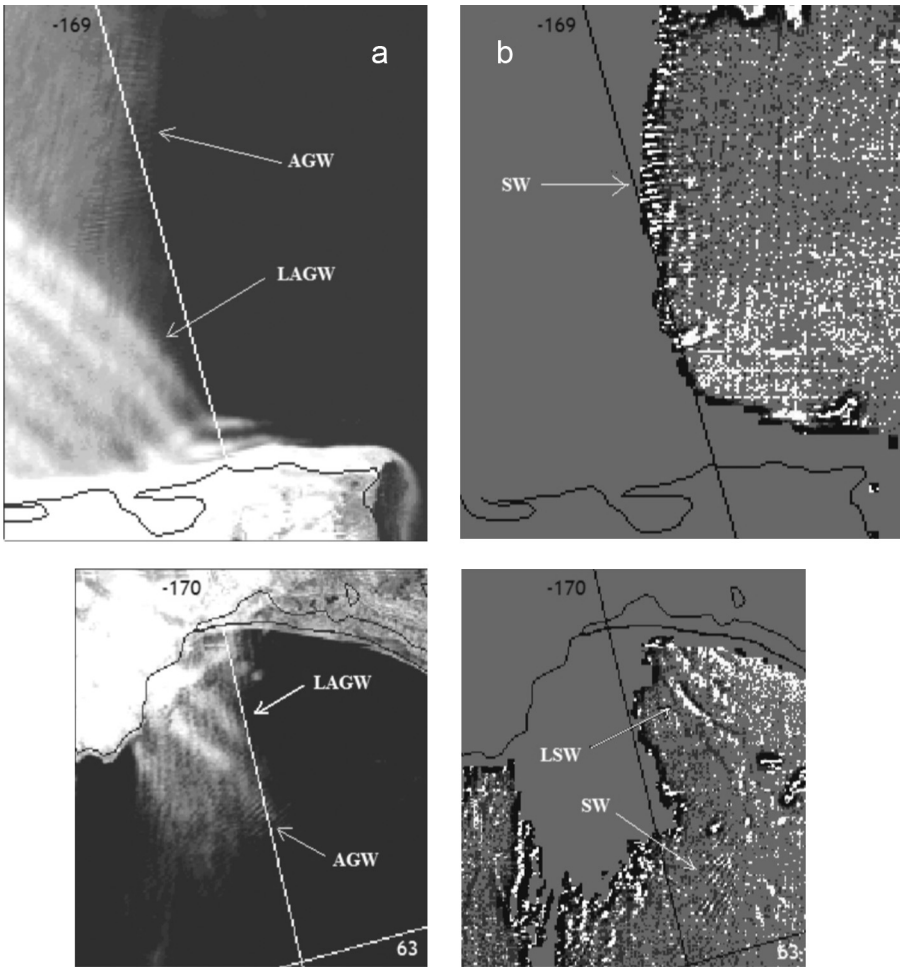

Figure 3 MODIS images: L_t(859) (a) and L_w(859) (b); upper — to the north and lower — to the south of St. Lawrence Island.

A small, southwestern AGW packet and a SW packet are visible on the L_t and L_w images. The packet width is no less than 23.6 km, the wave crest length is no less than 15 km, and the wavelength is 0.85 km. For both packets, SWs on L_w-images also appear to be like continuations of AGW cloudy signatures on L_t-images.

Images of $L_t(859)$ showed that cloudy waves of a smaller wavelength induced by AGWs were imposed on larger waves to the north and to the south from the island. This could be caused by different heights of AGWs in the low troposphere, so that cloudy waves were superimposed on each other on the image. Such phenomenon is observed frequently on satellite pictures and is also visible from the land.

The wind speed and direction were also calculated at 22:25 on 6 June 2001. A combined vector map is presented in Fig. 4. It is clear that the cold air outbreak with a wind speed of 11 m s^{-1} spread from the Arctic to the south. St. Lawrence Island was in the way of the stream and blocked it so that south from the island the wind speed did not exceed 8.5 m s^{-1} in the main stream. The island's blocking effect led to the origination of bow atmospheric waves that were directed to the north of the island against the air stream.

To disclose some peculiarities of the atmospheric–oceanic interactions, we represent the imposition in a difference mode of two images: $L_t(859)$ and $L_w(859)$ for a region of St. Lawrence Island (see Fig. 5). AGWs are shown in gray, and the crests of SWs that correspond to the highest L_w are shown in white. In Fig. 5 some combinations of SW crests (white arrows) and cloud stripes (black arrows) are presented.

In this paper, we present evidence that the surface waves were not long surface gravity waves but rather atmospheric wave imprint on the sea's surface. For this purpose, it is necessary to evaluate the phase speed of the atmospheric wave c_a and the speed of ocean surface gravity wave c_g that can propagate in the ocean of variable depth. c_a for the given site and time was calculated in Li et al. (2004) on the basis of the radiosonde upper air observation at nearby station Nome at Alaska at 12:00 on 6 June 2001. Using a forced, extended Korteweg-de Vries equation for a vertical profile of potential temperature, representing a two-layer system, the phase speed was evaluated as c_a = 8.9 m s^{-1} (Li et al., 2004). This

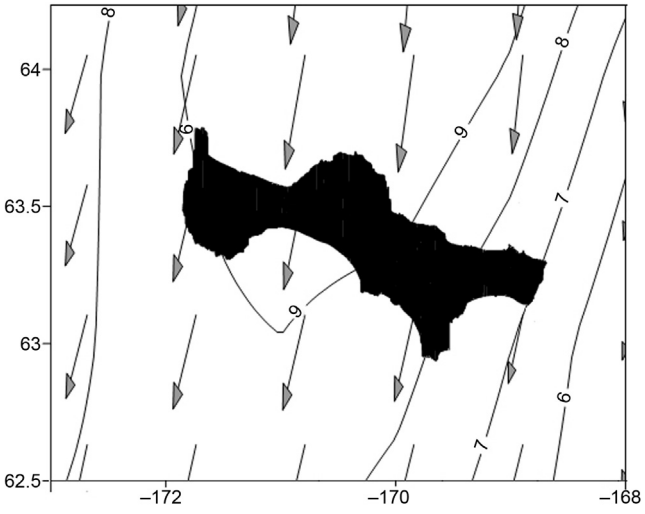

Figure 4 Wind speed (isolines) and wind direction (arrows) at a height of 10 m.

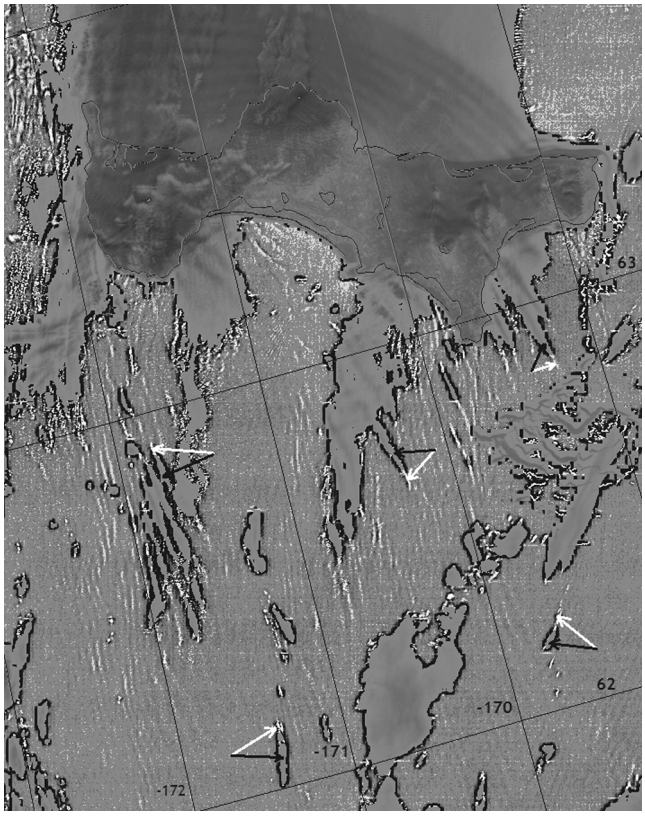

Figure 5 Imposition in a difference mode of $L_t(859)$ and $L_w(859)$ near St. Lawrence Island; some combinations of cloud-surface waves are denoted by black and white arrows.

value is close to the ocean wind speed near the island (see Fig. 4). As was shown previously, the wavelength of AGWs and SWs to the south of the island was from 1.5 km to 4 km. The depth in the region shown in Fig. 5 changes from h = 20 m near the island to h = 50 m near 62°N. When evaluating the phase speed for hypothetical surface gravity waves with a wavelength 1.5–4 km, we use an approximation of the dispersion relation for shallow waters, $c_g^2 = gh$, where g is the acceleration of gravity (Grimshaw et al., 1998). Calculations show that the speed c_g for such waves should be 14 m s^{-1} for the depth 20 m and 22 m s^{-1} for the depth 50 m, which is greater than the speed of AGWs. Moreover, as seen in Fig. 5, the locations of SW crests were generally like prolongations of AGW cloud imprints on the superimposed image, independent on depth, so we conclude that the SWs were exactly imprints of AGWs but not long gravity waves.

3.2. AGWs in the Gulf of Mexico

Another example of AGW imprints in clouds and on the sea surface was obtained with data from MODIS-Terra at 16:50 and MODIS-Aqua at 20:00 on 15 March 2008, in the Gulf of Mexico. A packet of atmospheric waves in the form of an undular bore was recorded as parallel white cloud stripes moving to the south. Desaturated true-color L_t-images of the bore are shown in the upper part of Fig. 6, on the left – obtained from MODIS-T and on the right – from MODIS-A. In the lower part of Fig. 6, the image of *Rrs*(859) of MODIS-A at 20:00 with increased brightness and contrast is shown. AGWs

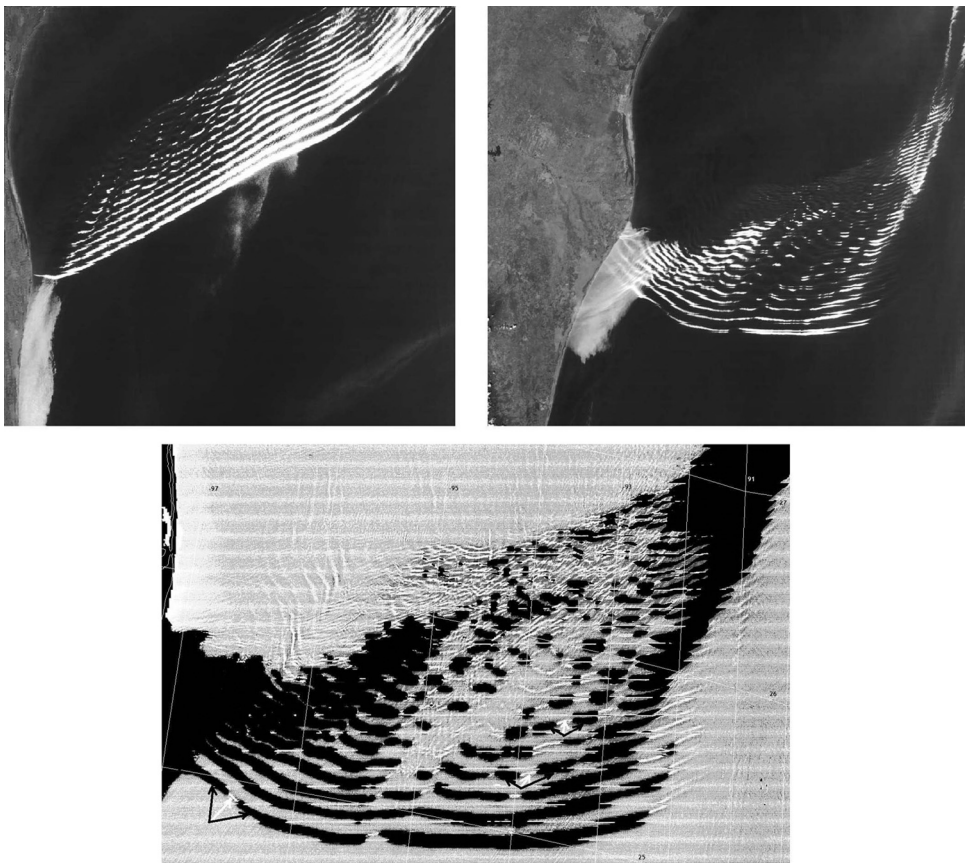

Figure 6 An undular bore wave packet in the Gulf of Mexico on 15 March 2008: above — desaturated true-color images of L_t, on the left — from MODIS-Terra at 16:50, on the right — from MODIS-Aqua at 20:00, below — a part of the increased *Rrs*(859) image at 20:00.

in clouds are presented in black and the crests of SWs in white. Some combinations of cloud-surface waves are denoted by black and white arrows. Defined by MODIS-T and MODIS-A data, the undular bore covered a distance of 83 km in 190 min. Thus the phase speed of AGWs was $c_a = 7\ \mathrm{m\ s^{-1}}$. The mean horizontal wavelength of AGWs defined by MODIS-A image was $\lambda_a = 10$ km, the same was the wavelength of surface waves λ_s. The depth h in the region varies from 100 m to 2000 m. As $h_{max} = 2$ km is no larger than a half of the wavelength λ_s, we used an approximation of the dispersion relation for shallow waters for evaluation of the phase speed of hypothetical long surface gravity waves (Grimshaw et al., 1998). For this case, $c_g = 30$—$140\ \mathrm{m\ s^{-1}}$, which is much greater than c_a. The crests of SWs were like prolongations of AGWs in clouds so we conclude that SWs could only be the imprints of AGWs, but not long gravity waves.

3.3. AGWs in the Carpentaria Gulf, Australia

One more example of AGWs and their impact on the sea surface is presented on the MODIS-Terra image obtained on 2 August 2002, at 01:00 in the Gulf of Carpentaria, to the north of Australia (sea Fig. 7). A desaturated, true-color

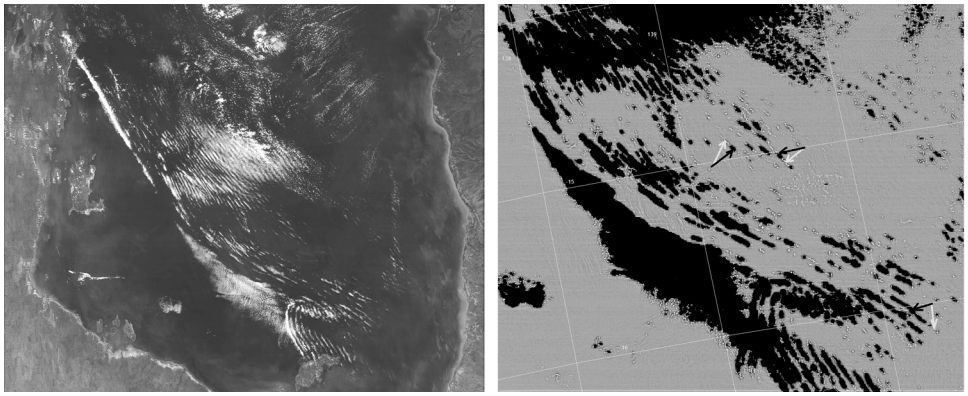

Figure 7 An undular bore on MODIS-Terra image obtained at 01:00 on 2 August 2002, in the Gulf of Carpentaria, Australia: on the left — a desaturated true-color image of L_t, on the right — a part of the increased *Rrs*(859) image.

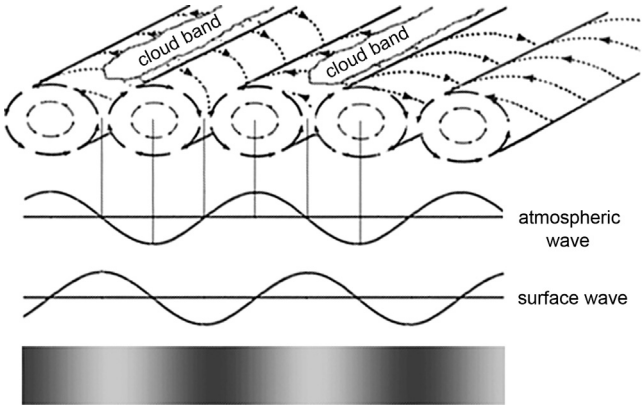

Figure 8 A scheme of the relative positioning of the AGW and the SW.

L_t-image of the gulf is shown on the left of Fig. 7. A typical phenomenon for this time of year is the Morning Glory — a powerful, solitary, low-level atmospheric wave that occurs as a roll cloud (shown in the left upper part of the image) with a number of waves. It represents an undular bore that appeared as parallel cloud stripes moving along the gulf. The image of *Rrs*(859) with increased brightness and contrast is presented on the right of Fig. 7. Cloudy AGWs are well defined as black stripes, and the crests of SWs as white stripes. The wavelength of AGWs and SWs was 7—10 km. SW crests were also like prolongations of the cloudy AGWs on the *Rrs*-image.

4. Discussion and conclusions

Thus, MODIS 250-m scanner returns at 859 nm are optimal for studying atmospheric waves by their traces in clouds and on the sea surface. These traces are mostly convenient to observe on ocean color scanner images in the case of intermittent cloudiness, when they imprint in adjacent parts of the region and are visible on a single satellite picture.

Signatures of AGWs propagating in the low troposphere were clearly manifested on images of normalized water leaving radiance L_w(859) (or remote sensing reflectance *Rrs*(859)). A studding of the nature of SWs was carried out. For this aim the phase speeds of AGWs were evaluated. On the basis of the wavelength of SWs and the values of variable ocean depth, the phase speeds of hypothetical ocean surface gravity waves were estimated in accordance with the dispersion relation, in the approximation of shallow waters. Evaluations showed that the phase speeds of hypothetical gravity waves should be much greater than the phase speeds of AGWs. Moreover, cloud imprints had prolongations in the crests of SWs. Therefore we conclude that the observed SWs could not be the long gravity waves but the imprints of AGWs. From this also follows that AGWs impact on the cloudy layer and on the sea surface instantly and simultaneously.

It is known from Gossard and Hooke (1975) that an AGW originates in a set of counter-rotating, nearly circular atmospheric vortices, so that the maximum and the minimum amplitudes of the AGW coincide with eddy axes. Between two adjacent, counter-rotating atmospheric vortices above the updraft part of the vortices' circulations, cloud bands can be formed, whereas sinking motions of atmospheric vortices correspond to areas free of cloud (Etling and Brown, 1993). Thus, if we consider the AGW, then cloud bands fit with areas where the AGW's vertical displacement is near zero (see the scheme in Fig. 8).

Figs. 5—7 show that the light stripes on L_w or *Rrs* images, which reflect the maximum amplitudes of AGWs, are a kind of prolongation of cloud stripes. This corresponds to a near zero displacement of AGWs so SWs were shifted by minus a quarter of the period relative to AGWs. This situation is shown on the scheme (Fig. 8) where cloud bands, reflected the AGW, and the SW, are presented in several projections. The scheme resembles a situation when a resonance of Proudman between AGWs and anemobaric waves on the ocean surface occurs (Levin and Nosov, 2009). From the cases considered, it follows that the resonant conditions are inherent for AGWs and their imprints on the sea surface in the form of SWs. Similar signatures are found to be manifested on L_w or *Rrs* images with a high spatial resolution obtained from MODISes flown on two NASA spacecrafts (Terra and Aqua) in different areas of the World Ocean regardless on depth.

Acknowledgement

This work is supported by grant of Russian Foundation for Basic Research N 08-05-00298-a.

References

Alpers, W., Brummer, B., 1994. Atmospheric boundary layer rolls observed by the synthetic aperture radar aboard the ERS-1 satellite. J. Geophys. Res. 99 (C6), 12613—12621.

Alpers, W., Huang, W., 2011. On the discrimination of radar signatures of atmospheric gravity waves and oceanic internal waves on synthetic aperture radar images of the sea surface. IEEE Trans. Geosci. Remote Sens. 49 (3), 1114—1126.

Da Silva, J., Magalhaes, J., 2009. Satellite observations of large atmospheric gravity waves in the Mozambique Channel. Int. J. Remote Sens. 30 (5), 1161—1182.

Etling, D., Brown, R., 1993. Roll vortices in the planetary boundary layer: a review. Bound.-Lay. Meteorol. 65 (3), 215—248.

Evdoshenko, M., 2008. Imprints of atmospheric events on the Caspian Sea surface by MODIS high resolution data. In: Proc. 9th Pan Ocean Remote Sensing Conf. (PORSEC 2008), Ocean Manifestation of Global Changes, 2—6 December 2008, Guangzhou, China, p. 42.

Evdoshenko, M., 2009. Using of MODIS high resolution data for study of atmospheric processes by their imprints on the sea surface. In: Proc. 4th Workshop on Remote Sensing of the Coastal Zone, Coasts and Climate Conflicts, 18—20 June 2009, Chania, Crete, Greece.

Franz, B., Werdell, P., Meister, G., Kwaitkowska, E., Bailey, S., Ahmad, Z., McClain, C., 2006. MODIS land bands for ocean remote sensing applications. In: Proc. Ocean Optics Conf. XVIII, 9—13 October 2006, Montreal, Canada.

Gordon, H., Brown, O., Evans, R., Brown, J., Smith, R., Baker, K., Clark, D., 1988. A semi-analytical radiance model of ocean color. J. Geophys. Res. 93 (D9), 10909—10924.

Gossard, E., Hooke, W., 1975. Waves in the Atmosphere: Atmospheric Infrasound and Gravity Waves — Their Generation and Propagation. Elsevier Sci. Publ., Amsterdam, 472 pp.

Grimshaw, R., Ostrovsky, L., Shrira, V., Spepanyants, Yu., 1998. Long nonlinear surface and internal gravity waves in a rotating ocean. Surv. Geophys. 19 (4), 289—338.

Hale, G., Querry, M., 1973. Optical constants of water in the 200-nm to 200-m wavelength region. Appl. Optics 12 (3), 555—563.

Kozlov, I., Romanenkov, D., Zimin, A., Chapron, B., 2014. SAR observing large-scale nonlinear internal waves in the White Sea. Remote Sens. Environ. 147, 99—107.

Levin, B., Nosov, M., 2009. Physics of Tsunamis. Springer Science & Business Media V.M., New York, 327 pp.

Li, X., Dong, X., Clemente-Colón, P., Pichel, W., Friedman, K., 2004. Synthetic aperture radar observation of the sea surface imprints of upstream atmospheric solitons generated by flow impeded by an island. J. Geophys. Res. 109, C02016.

Li, X., Zheng, W., Yang, X., Li, Z., Pichel, W., 2011. Sea surface imprints of coastal mountain lee waves imaged by synthetic aperture radar. J. Geophys. Res. 116, C02014.

Li, X., Zheng, W., Zou, C.-Z., Pichel, W., 2008. A SAR observation and numerical study on ocean surface imprints of atmospheric vortex streets. Sensors 8 (5), 3321—3334.

Liu, A.Q., Moore, G.W.K., Tsuboki, K., Renfrew, I.A., 2004. A high-resolution simulation of convective roll clouds during a cold-air outbreak. Geophys. Res. Lett. 31, L03101.

Pegau, W., Gray, D., Zaneveld, J., 1997. Absorption and attenuation of visible and near-infrared light in water: dependence on temperature and salinity. Appl. Optics 36 (24), 6035—6046.

Vachon, P.W., Johannessen, O.M., Johannessen, J., 1994. An ERS 1 synthetic aperture radar image of atmospheric lee waves. J. Geophys. Res. 99 (11), 22483—22490.

Valenzuela, G.R., 1978. Theories for the interaction of electromagnetic and oceanic waves: a review. Bound.-Lay. Meteorol. 13 (1), 61—85.

Weigen, X., Xilin, G., Li, X., 2008. Coastally trapped atmospheric gravity waves on SAR, AVHRR and MODIS images. Int. J. Remote Sens. 29 (6), 1621—1634.

Zheng, Q., Yan, X.-H., Klemas, V., Ho, C.-R., Kuo, N.-J., Wang, Z., 1998. Coastal lee waves on ERS-1 SAR images. J. Geophys. Res. 103 (C4), 7979—7993.